Nanoparticles by ICP-RF plasma

Haye, Emile; Busby, Yan; Bocchese, Florian; Da Silva Pires, Mathieu; Pireaux, Jean-Jacques; Houssiau, Laurent

Published in:
Belvac News

Publication date:
2018

Nanoparticles by ICP-RF plasma: a versatile process to synthesize tuneable nanoparticles

Emile HAYE, Yan BUSBY, Florian BOCCHESE, Mathieu DA SILVA, Jean-Jacques PIREAUX, Laurent HOUSSIAU.

Laboratoire Interdisciplinaire de Spectroscopie Electronique, Namur Institute of Structured Matter, Rue de Bruxelles 61, 5000-Namur.

Corresponding authors :
emile.haye@unamur.be
yan.bubsy@unamur.be

Abstract

To explore new routes for the synthesis of efficient, durable and low-impact catalyst materials is highly desirable and urgent to face the so-called energetic transition. In this work we present a new approach for the metal/carbon catalyst synthesis based on low-pressure plasma treatment of a powder mixture comprising a high-surface area carbon support and an organometallic precursor. These catalysts materials have been recently demonstrated as a highly-versatile and eco-friendly for applications in proton exchange membrane (PEM) fuel cells. Compared to conventional chemical fabrication, plasma processing offers the advantage of reducing the environmental impact of the catalyst by reducing the energy consumption and relying on a solvent-free waste-free scalable process. We investigated the nucleation process of Pt Ni and Co nanoparticles, under different plasma discharge conditions (power, time) and plasma composition (O, Ar and N-based plasmas) to affect the catalyst morphology and the chemical state of metal nanoparticles. Catalysts have been systematically characterized by analytical methods. Moreover we have explored the deposition of bimetallic Pt-Ni and Pt-Co nanocatalysts showing that the simultaneous or the sequential treatment of the two metal precursors leads to very different catalyst morphologies.

1. Introduction

Nanocatalysts based on metal nanoparticles deposited on nanostructured materials are widely used in electrochemical and energy devices such as fuel cells, gas sensors or electrolysers for water splitting.[1–5] In such applications, noble metals such as gold or platinum are reference material due to their superior electrochemical mass activity; however they are rare, expensive and have a high environmental impact (environmental pollution and toxicoly). [6,7] Low-cost “green” catalysts based on metal-free or non-noble materials have thus recently attracted intense research meant to reduce the cost and the environmental impact. In addition, the (partial) substitution or alloying of noble metal with non-noble metals has led to an enhancement of the catalytic properties, which highly depend of the non-noble metal properties and oxidation state. Among them, nickel and cobalt based nanomaterials exhibit promising properties both as metallic, oxide or nitride nanoparticles.[2,8,9]

Several Belgian research groups are involved in the synthesis of nanomaterials for energy applications. Among them, the Laboratoire Interdisciplinaire de Spectroscopie Electronique (LISE) at UNamur has developed in the last years a new synthesis method based on low-pressure RF plasma treatments. This methodology is particularly versatile to synthesize nanoparticles on high surface area carbon substrates such as carbon xerogels, graphene-based materials or carbon nanotubes. In particular, we applied different plasma conditions (RF power, treatment time, plasma composition, etc.) to treat different organometallic

precursors as reported in recent publications.[3,5,10] In this work, we present an overview of the different ways to synthesize controlled metal nanoparticles with a tuneable chemical state on different carbon substrates.

2. Materials and methods

The plasma-based processing of nanocatalysts starts by mixing a carbon powder precursor (carbon xerogel, carbon nanotubes or graphene) and an organometallic powder (Pt, Ni, Mn or Co acetylacetonate). Then, the mixture is introduced in an inductively coupled plasma radio frequency (ICP-RF) plasma reactor; this reactor is pumped down to high vacuum, then the plasma composition is regulated by injecting a controlled flow of gas mixture comprising Ar, O_2, N_2, NH_3, to reach a working pressure of few mTorr. The plasma discharge power is varied between 80 and 200 W.[3,5,10] The three key parameters of the process are (i) the choice of the carbon and the organometallic precursors, (ii) the choice of the injected plasma gas and (iii) the plasma power and treatment time. The different steps of the process are presented in **Figure 1**. The total duration of the treatment, generally between 15 and 60 min, depends on the time needed to decompose the organometallic precursors which depends on the discharge power.

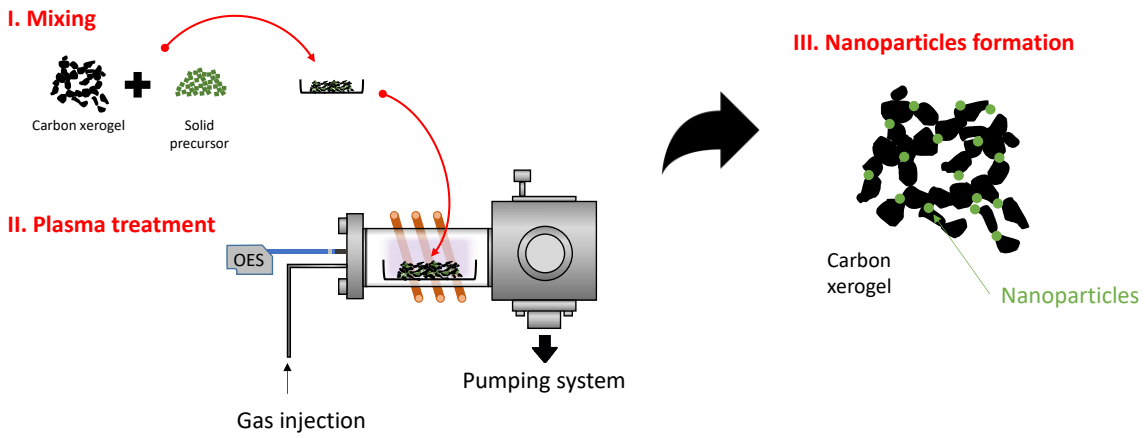

Figure 1 *– Schematic view of the different steps of the plasma processing of nanocatalysts.*

Optical emission spectroscopy (OES) measurements are performed during the plasma treatment, to monitor the precursor decomposition and the subsequent nanoparticle formation. The measurements are performed using an OceanOptics USB 4000XR spectrometer. After plasma treatment, the surface chemistry, the morphology and the crystal structure of the metal nanoparticles have been determined by X-ray photoelectron spectroscopy (XPS, K-Alpha spectrometer by Thermo Scientific), transmission electron microscopy (TEM, Philips Teknai 10) and X-ray diffraction (Pananalytical X'pert Pro) measurements. **Table 1** summarizes the different plasma conditions and precursors which were tested: the effect of the plasma power and composition have been investigated for Ni-based nanoparticles, considering three different plasma compositions (Ar:O_2, Ar:N_2 and Ar:NH_3) and plasma power from 80 to 200 W.[10] Investigations have been also carried out on Pt-based nanoparticles, considering three different atmospheres (Ar, O_2 and Ar/O_2) at 30 and 100 W, and in a two steps (low-energy / high-energy) plasma treatments.[3,5] Namely, the first step consists on a pulsed plasma treatment (40 min at 80 W, duty cycle 50%, frequency 10 Hz) followed by a short and more energetic continuous plasma treatment (100 W for 8 min and 150 W for 5 min). Bimetallic Pt-

Ni nanocatalysts have also been investigated: in particular we explored a simultaneous or sequential treatment of the two precursors. Finally, investigations are currently carried out on cobalt based nanoparticles. In our experiments the working pressure is between 5 and 10 mTorr for all treatments; this moderate pressure variation does not significantly influences the intensity of the plasma and the related organometallic precursor decomposition and nanoparticles nucleation.

Table 1 *– Overview of the different plasma conditions and organometallic precursors. The total gas flow is fixed between 5 and 10 sccm.*

Precursor	Injected Gas mixture	Plasma Discharge Power
$Pt(acac)_2$	Ar/O_2	2 steps treatment at low and high power
	O_2	30-100W
	Ar	30-100W
$Ni(acac)_2$	Ar/O_2	90-120-140-200W
	Ar/N_2	90-120-140-200W
	Ar/NH_3	90-120-140-200W
$Co(acac)_3$	Ar/NH_3	80-140-200W
	NH_3/O_2	80-140-200W
$Ni(acac)_2$ + $Pt(acac)_2$	O_2	2 steps treatment at low and high power
$Ni(acac)_2$ then $Pt(acac)_2$	O_2	2 steps treatment at low and high power
$Co(acac)_3$ + $Pt(acac)_2$	NH_3/O_2	80-140W
$Co(acac)_3$ then $Pt(acac)_2$	NH_3/O_2	80-140W

3. Results and Discussions

3.1 Monitoring of the organometallic precursor degradation

The plasma decomposition of the metal acetylacetonate and the subsequent nucleation of nanoparticles formation can be monitored by *in situ* OES measurements by looking at specific emission lines associated with the precursor decomposition. Optical emission spectra are acquired in the range between 200 and 900 nm; the typical spectra obtained at the beginning of the treatment with different plasma composition are reported in **Figure 2**.a. In the range between 680-895 nm and 395-435 nm, emission spectra are dominated by argon lines (Ar I) while when nitrogen species are present (N_2 or NH_3), additional lines appear between 310 and 390 nm, corresponding to the N_2 C-B lines and the CN violet system (emission lines at 386.7 and 388.2 nm);[11,12] when O_2 is injected into the plasma discharge, OH related emission lines are observed at 306.7, 309.2 and 313.6 nm (A-X lines[11]). Whatever the precursor, no emission lines coming from the metal (neutral or ions) have been observed.

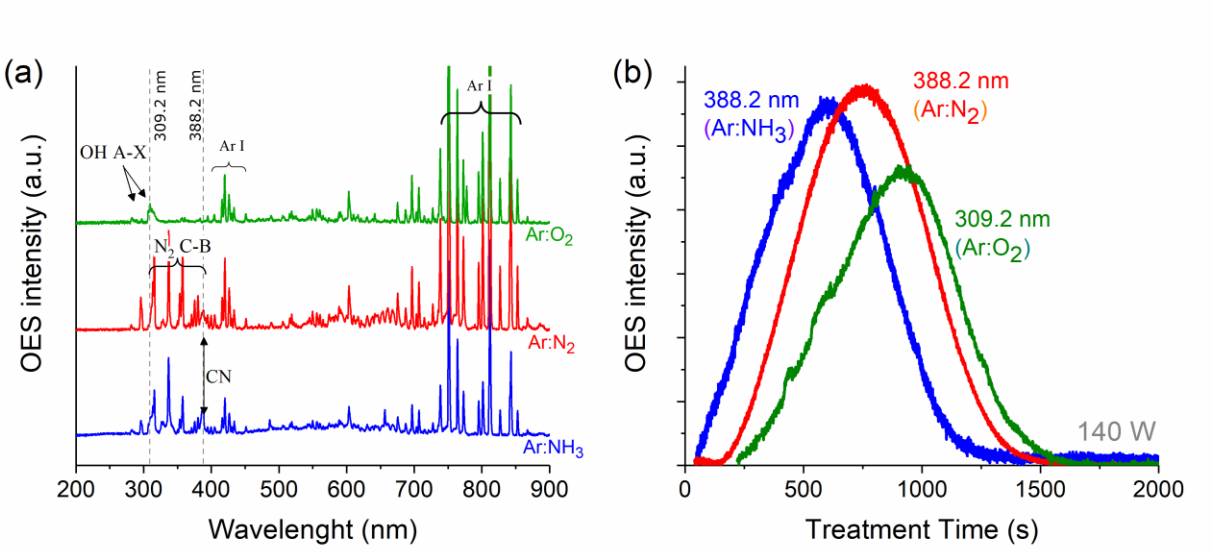

Figure 2 *- (a) OES spectra acquired in situ at the initial stage of a nitrogen-based (Ar:N_2 and Ar:NH_3) and oxygen-based (Ar:O_2) plasma treatments. Characteristic lines of the organometallic precursor decomposition are identified and followed in situ. (b) Evolution of the selected OES signals associated with the decomposition of the organometallic precursor in the different plasma environments: for Ar:N_2 and Ar:NH_3 plasmas, the OES signal at 388.2 nm (CN emission lines) is selected while for the Ar:O_2 plasma we follow the signal at 309.2 nm (OH emission lines).*

The intensity of the Ar-related emission lines remains constant during the treatment, while other lines exhibit a clear intensity rise and fall along the plasma treatment making them good candidates to be associated to the decomposition of the precursor: among them, we have selected the most intense lines to monitor *in situ* the precursor decomposition. In nitrogen and ammonia-based plasmas, we select the CN line at 388.2 nm emission, while for Ar:O_2 plasma, the OH line at 309.2 nm is chosen. The rise and fall behaviour of these signal intensities in a 140 W plasma treatment are shown in **Figure 2**.b. It is clear that, depending on the plasma atmosphere, the decomposition occurs at different rates, that have been investigated trough a kinetic model.[10] The decomposition of the precursor is also dependent to the plasma power, as shown on **Figure 3**: not surprisingly, as the power increase, the full decomposition time decreases.

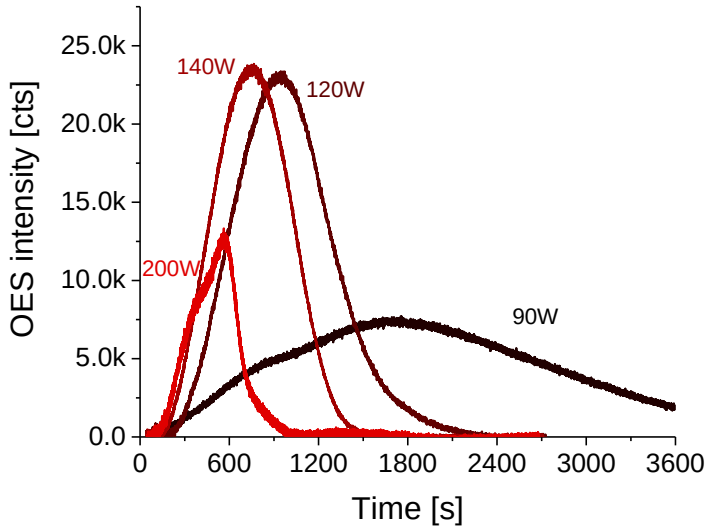

Figure 3 *– Evolution of the selected OES signal (CN emission line at 388.2 nm) as a function of time for Ar:N_2 treatment at different power for the sample containing the Ni precursor. As the power increases, the time required for the precursor decomposition decreases.*

The direct correlation between the drop of these specific OES signals and the precursor decomposition is confirmed by acquiring *ex situ* XRD spectra at regular treatment time steps, showing the progressive disappearance of the XRD pattern related to the (crystalline) $Ni(acac)_2$ precursor (**Figure 4**).

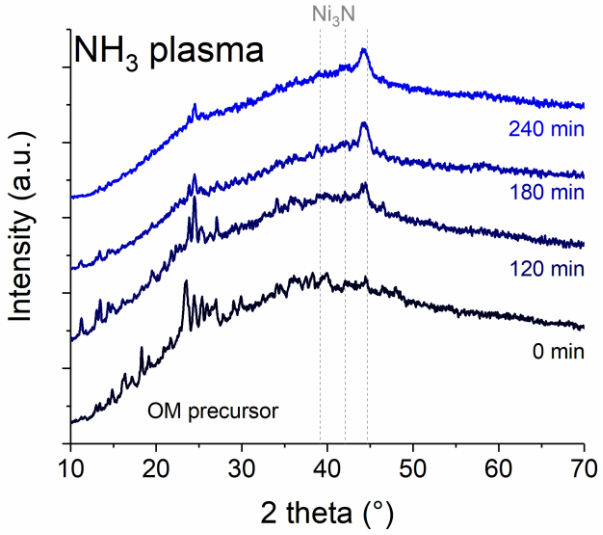

Figure 4 *– XRD spectra of the samples containing the carbon support and the Nickel precursor before treatment, and after NH_3 treatment at different time. The diffraction peaks of the crystalline precursor disappear as the treatment occurs, while Ni_3N nanoscale domains are clearly formed.*

3.2 Amorphous or crystallized nanoparticles?

For each explored metal precursors (Pt, Ni, Co acetylacetonate), as its specific XRD pattern disappears, we have observed the formation of nanoparticles in TEM/STEM images (Figure 5). For most of the cases, the nanoparticles are dense and homogeneously dispersed on the carbon substrate, the size distribution is unimodal, with size ranging from 1 up to 8 nm depending on the treatment conditions. The nanoparticles size is mainly affected by the plasma power and the treatment time: long and high-power treatments will facilitate the

diffusion of atoms and of small metal cluster that will participate to the formation of larger nanoparticles in order to minimize their surface energy.

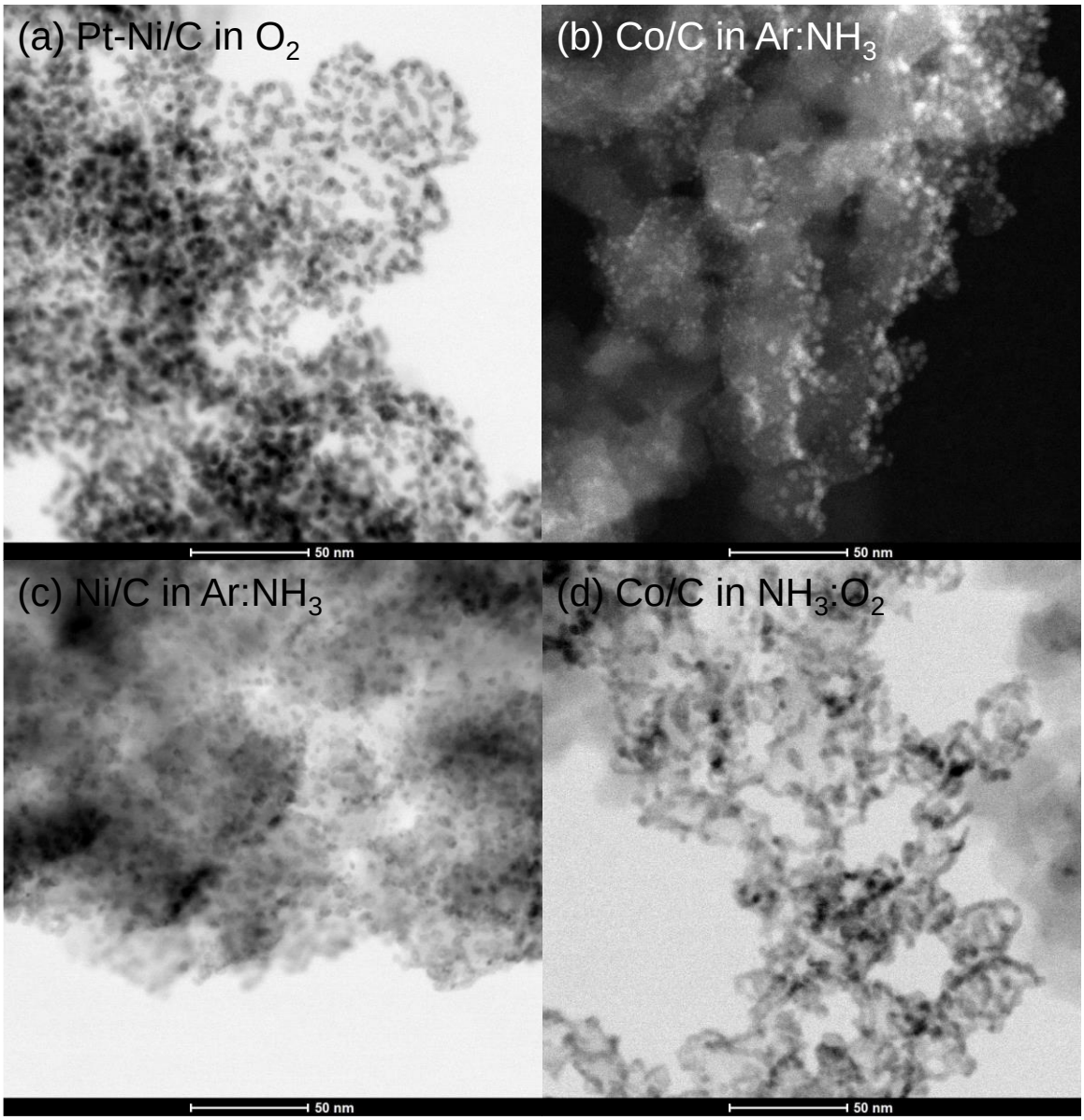

Figure 5 *– Scanning transmission electron microscopy (STEM) of (a) Pt-Ni/C treated in O_2 plasma, (b) Co/C treated in Ar:NH_3 plasma, (c) Ni/C treated in Ar:NH_3 plasma and (a) Co/C treated in NH_3:O_2 plasma.*

The structure and morphology of the nanoparticles generally depend on the precursor, the plasma composition and the power. Platinum generally forms crystallized nanoparticles, with a significant signal observed on XRD patterns at 39.2, 45.6 and 66.5° corresponding to (111), (200) and (220) diffraction peaks (**Figure 6**). For non-noble metals such as nickel and cobalt, the particles nucleation displays a different behaviour, much more dependent of the plasma power and atmosphere. For example, inert or oxidising plasma gas mixtures (Ar, N_2 or O_2) result in the formation of amorphous nanoparticles (**Figure 6**.c and d), except for very high power conditions (200 W), for which slightly crystallized nanodomains appear.

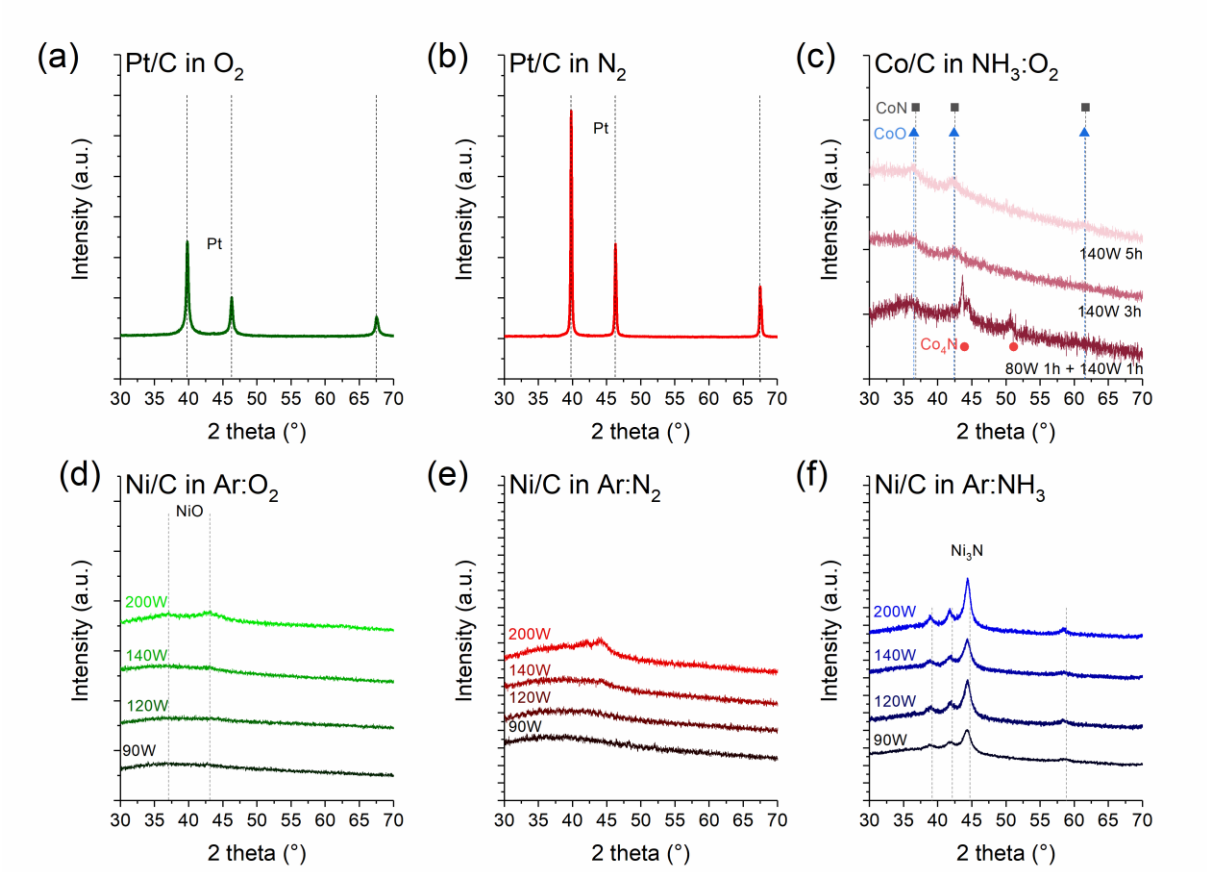

Figure 6 *– XRD patterns recorded after treatment of different precursors mixed with carbon substrate: Pt/C after treatment in (a) O_2 plasma, (b) N_2 plasma; Co/C after treatment in (c) NH_3:O_2 plasma; Ni/C after treatment in (d) Ar:O_2 plasma, (e) Ar:N_2 plasma and (f) Ar:NH_3 plasma*

The introduction of a reducing plasma gas such as ammonia leads to the formation of crystallized non-noble metal nitride nanoparticles (**Figure 6**.f). Cobalt and nickel precursors behave similarly (not shown here) and their decomposition has been studied in NH_3:O_2 plasmas (**Figure 6**.c). In such an atmosphere, where both oxidising and reducing agents are present, the nucleation mechanisms is particularly complex and it is still under investigations. Preliminary results indicate that different domains nucleate depending on the treatment time: some cobalt nitrides with a low nitrogen content (Co_4N) appear first, and then, evolve during the treatment time to form N-rich or O-rich domains (CoN or CoO).

3.3 Metallic, oxidized (or nitride) nanoparticles?

After plasma treatments of $Pt(acac)_2$, XPS analysis shows the presence of different oxidation states depending on the plasma conditions. In ammonia-based plasma a strong contribution from Pt^0 is observed in the Pt 4f spectra at 71.2 eV binding energy (BE) (**Figure 7**.a),[13] while a larger Pt^{2+} at 72.4 eV BE attributed to Pt^{2+} is observed when oxygen is introduced into the reactor (**Figure 7**.b). In opposite, non-noble metal precursors result in the systematic formation of a strong oxide component that can be lowered by introducing a reducing agent such as ammonia or by increasing the power (**Figure 7**.c and d). The use of inert gasses (Ar or N_2) is not sufficient to avoid the formation of oxides probably because of the presence of oxygen in the organic part of the precursor and on the plasma reactor. The presence of oxides is evidenced on Ni 2p and Co 2p core level spectra generally showing strong contributions from

Ni^{2+}, Ni^{3+}, Co^{2+} and Co^{3+} (Figure 7.c and 7.d). The increase of plasma power, in presence of oxygen or nitrogen leads to a slight reduction of oxidation, as evidenced by the decrease of Ni^{2+} and Ni^{3+} and the increase of Ni^{0} contribution (**Figure 7**.c). This effect is attributed to the preferential erosion of oxygen by Ar^{+} species at high discharge power.[14]

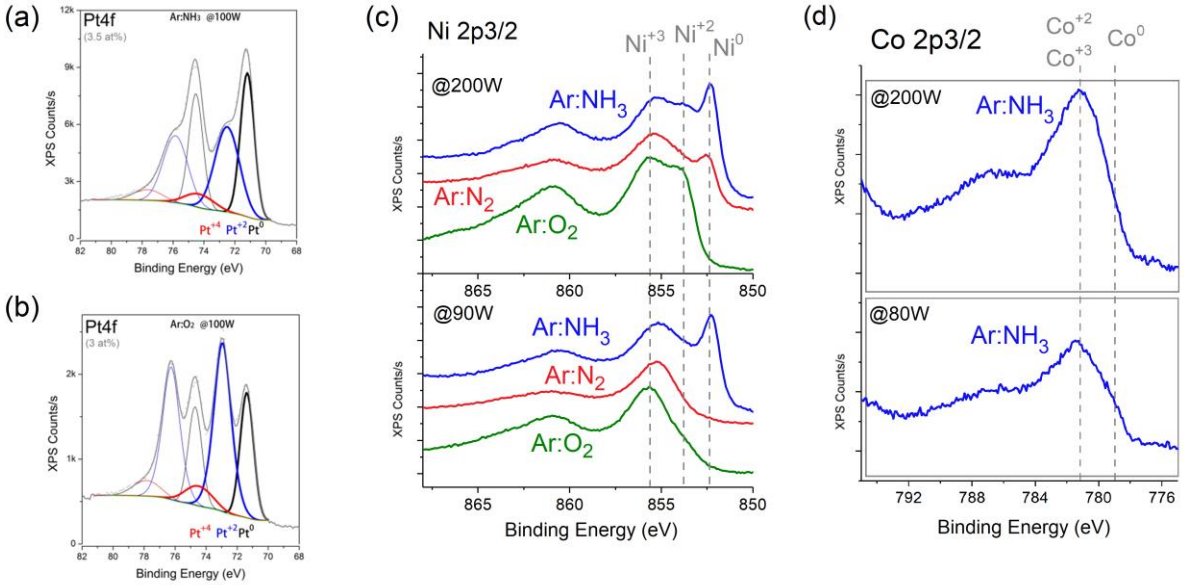

Figure 7 *– XPS measurements of different plasma treated samples: Pt 4f core level spectra after (a) Ar:NH_3 and (b) Ar:O_2 treatments at 100 W. (c) Ni 2p 3/2 core level spectra for Ar:NH_3, Ar:N_2 and Ar:O_2 treatments at 90 and 200 W. (d) Co 2p 3/2 core level spectra for Ar:NH_3, treatments at 80 and 200 W.*

3.4 Formation of bimetallic nanoparticles

In order find strategies to reduce the amount of noble metal into the catalyst, we have explored the synthesis of bimetallic Pt-Ni nanocatalysts. The synthesis of bimetallic particles is simply achieved by treating the two metal precursors, either sequentially (before the Ni precursor, then the Pt precursor) or simultaneously. Both treatment conditions have been explored on a graphene substrate and by using oxygen plasma (**Figure 8**). The morphology and the chemistry of the nanocatalysts have been characterized by EDS-STEM measurements and revealed a very different nanoparticle formation mechanism.

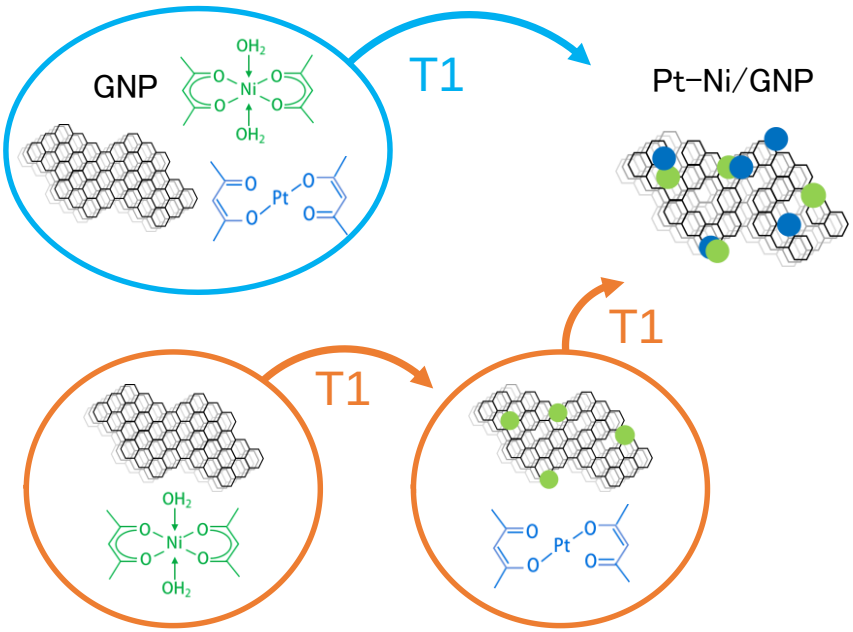

Figure 8 *- Sketch of the two strategies for the plasma deposition of Pt-Ni/GNP catalysts. T_1 corresponds to the simultaneous treatment, while T_2 represents the sequential treatment.*

In the simultaneous treatment condition (T_1), the final composite morphology is rather complex; the high-resolution TEM image shown in **Figure 9**.a indicates that some nanoparticles display fringes from crystallographic planes while other particles characterized by a different contrast in STEM images do not show these fringes. The nanoparticles size distribution is rather wide going from 1 up to 6 nm. Complementary investigations with high angle annular dark field (HAADF) STEM in **Figure 9**.**Error! Reference source not found.**b confirm the very complex while reproducible morphology characterized by nanostructured domains up to 10 nm. Different atomic numbers result in a pronounced greyscale contrasts in STEM images, so the strong contrast variation in **Figure 9**.b suggests some compositional differences among interrelated nanoscale domains. This is confirmed by high-resolution EDS maps clearly showing that both Ni and Pt species form interconnected domains.

Results are very different for the sequential treatment of the precursors (T_2); the first treatment of the Ni precursor leads to the formation of homogeneously dispersed and well-defined Ni nanoparticles with an average size of 1.7 ±0.6 nm (**Figure 9**.c) and few larger particles probably resulting from the particles coalescence. After the addition of the Pt precursor and the second treatment, the nanoparticles exhibit a similar morphology with a slightly larger average particle size, from 1.7 to 2.1 nm (**Figure 9**.d). Interestingly, no additional particles coalescence is observed, while the nanoparticles display an increasing contrast in TEM images. This fact together with limited increase of the particle size and density suggests that Pt particles tend to nucleate preferentially on Ni particles acting as germination sites.[15,16] The Pt nanoparticles binding to Ni particles hinders their coalescence even at under energetic plasma treatment conditions (i.e. RF power >100 W). The rather small particle size does not allow discriminating whether Pt tends to form a shell over the Ni core or just to form attached particles. The different composite morphologies suggest that two kinds of nucleation mechanisms occur: during the simultaneous degradation of the two organometallic precursors (T_1), the particles nucleation starts on anchoring sites on the carbon surface such as defects on the graphene lattice or on oxygen based functional groups,[3] while during the sequential treatments (T_2), Pt particles start to nucleate on Ni seeds resulting in more defined particles: more in details, our interpretation is that while anchoring defects are generated by the plasma

on the graphene layer, the ionized molecules from the Pt precursor would preferentially bind to active sites on Ni particles to successively lead to the formation of bimetallic Pt-Ni particles. The complex morphology induced by the simultaneous treatment T_1 suggests the presence of multiple interrelated particle formation mechanisms involving the formation of carbon defects on the graphene sheets,[3] the absorption of oxygen, the nucleation of metallic particles, the formation of active defects on the particles surface, etc.

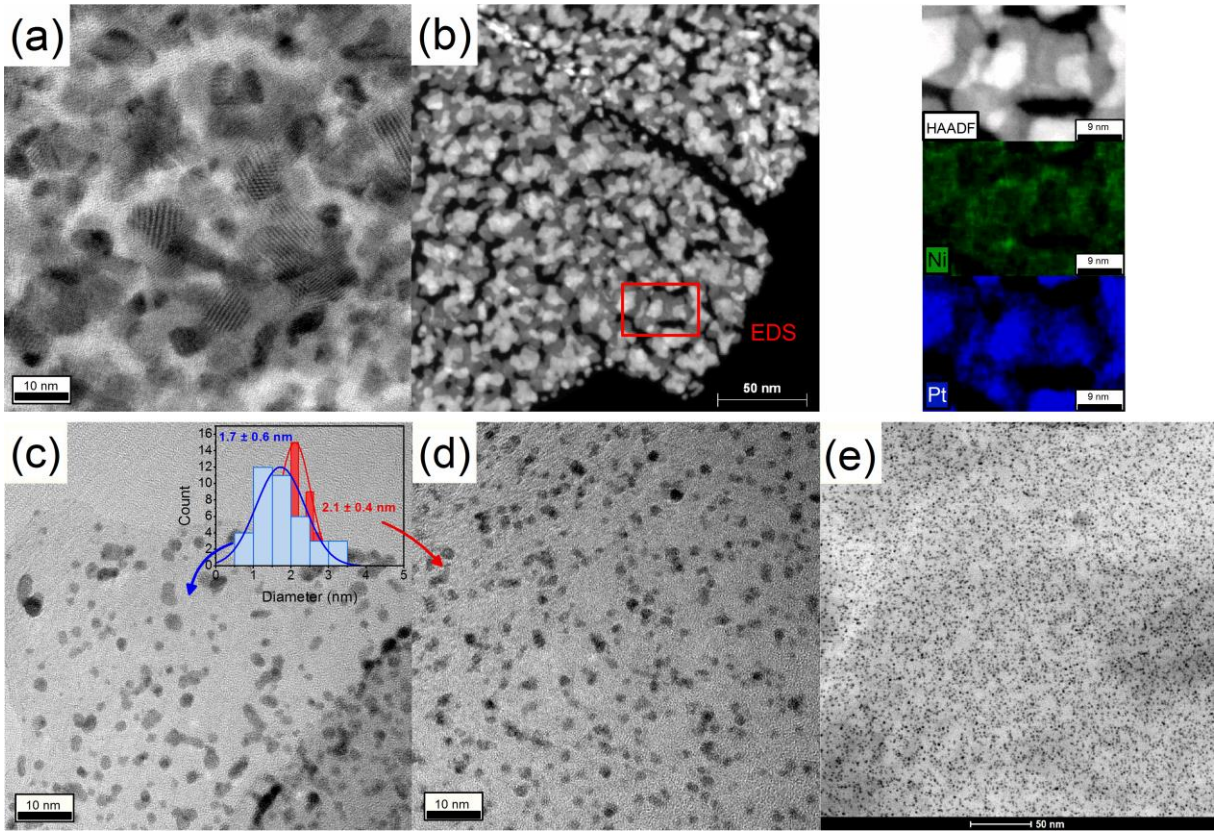

Figure 9 *- Characterization of the Pt-Ni composites made following a simultaneous treatment: (a) TEM, (b) HAADF and EDS mapping. (c) TEM image acquired after the first plasma treatment of the Ni precursor (d) TEM image acquired after the second plasma treatment of the Pt precursor (e) STEM image at the end* T_2.

Conclusion

A versatile process based on low-pressure plasma treatments has been described for the tuneable synthesis of metal nanoparticles. The process consists in the mixing of powder precursors which are treated in a RF ICP plasma under different atmospheres varied by selecting the injected gas mixture. Depending on the precursors and the plasma conditions, the nanoparticle size, structure, and chemical state can be tailored to meet specific requirements. In addition, the precursor decomposition and the subsequent nanoparticle formation can be *in situ* monitored by OES.

The treatment on noble metal precursor such as $Pt(acac)_2$ systematically leads to the formation of crystallized and strongly metallic nanoparticles, even when using an oxygen plasma. In opposite, the treatment of non-noble metal precursors such as $Ni(acac)_2$ and $Co(acac)_3$ generally results in the formation amorphous strongly oxidized nanoparticles. The

oxidation can be limited using high power treatment using reductive (ammonia) plasma treatments. Finally, the synthesis of bimetallic nanoparticles is reported: for Pt-Ni nanoparticles on graphene flakes, results were very different depending on the treatment conditions of the two precursors: namely, the sequential or simultaneous treatments resulted in very different catalyst morphologies. In particular, while Pt, Ni and Ni oxide nanodomains are formed in a simultaneous treatment, Pt particles attached on the previously formed Ni core particles are formed in a sequential treatment. These results demonstrate the high potential of low-pressure plasma to deposit tuneable green catalyst materials for many different applications in energy and catalysis.

References

(1) Shalom, M.; Ressnig, D.; Yang, X.; Clavel, G.; Patrick Fellinger, T.; Antonietti, M. Nickel Nitride as an Efficient Electrocatalyst for Water Splitting. *J. Mater. Chem. A* **2015**, *3*, 8171–8177.

(2) Metin, Ö.; Mazumder, V.; Özkar, S.; Sun, S. Monodisperse Nickel Nanoparticles and Their Catalysis in Hydrolytic Dehydrogenation of Ammonia Borane. *J. Am. Chem. Soc.* **2010**, *132*, 1468–1469.

(3) Laurent-Brocq, M.; Job, N.; Eskenazi, D.; Pireaux, J.-J. Pt/C Catalyst for PEM Fuel Cells: Control of Pt Nanoparticles Characteristics through a Novel Plasma Deposition Method. *Appl. Catal. B Environ.* **2014**, *147*, 453–463.

(4) Alonso, F. Nickel Nanoparticles in the Transfer Hydrogenation of Functional Groups. *RSC Catal. Ser.* **2014**, *17*, 83–98.

(5) Busby, Y.; Stergiopoulos, V.; Job, N.; Pireaux, J. J. Low Pressure Plasma Synthesis of Pt/C Catalysts for Fuel Cells Applications. **2016**.

(6) Maboeta, M. S.; Claassens, S.; Rensburg, L. van; Rensburg, P. J. J. van. The Effects of Platinum Mining on the Environment from a Soil Microbial Perspective. *Water. Air. Soil Pollut.* **2006**, *175*, 149–161.

(7) Gagnon, Z. E.; Newkirk, C.; Hicks, S. Impact of Platinum Group Metals on the Environment: A Toxicological, Genotoxic and Analytical Chemistry Study. *J. Environ. Sci. Health Part A Tox. Hazard. Subst. Environ. Eng.* **2006**, *41*, 397–414.

(8) Yu, D.; Zhang, X.; Wang, K.; He, L.; Yao, J.; Feng, Y.; Wang, H. Sawtooth-Shaped Nickel-Based Submicrowires and Their Electrocatalytic Activity for Methanol Oxidation in Alkaline Media. *Int. J. Hydrog. Energy* **2013**, *38*, 11863–11869.

(9) Carnes, C. L.; Klabunde, K. J. The Catalytic Methanol Synthesis over Nanoparticle Metal Oxide Catalysts. *J. Mol. Catal. Chem.* **2003**, *194*, 227–236.

(10) Haye, E.; Busby, Y.; da Silva Pires, M.; Bocchese, F.; Job, N.; Houssiau, L.; Pireaux, J.-J. Low-Pressure Plasma Synthesis of Ni/C Nanocatalysts from Solid Precursors: Influence of the Plasma Chemistry on the Morphology and Chemical State. *ACS Appl. Nano Mater.* **2017**.

(11) Machala, Z.; Janda, M.; Hensel, K.; Jedlovský, I.; Leštinská, L.; Foltin, V.; Martišovitš, V.; Morvová, M. Emission Spectroscopy of Atmospheric Pressure Plasmas for Bio-Medical and Environmental Applications. *J. Mol. Spectrosc.* **2007**, *243*, 194–201.

(12) Cvelbar, U.; Krstulović, N.; Milošević, S.; Mozetič, M. Inductively Coupled RF Oxygen Plasma Characterization by Optical Emission Spectroscopy. *Vacuum* **2007**, *82*, 224–227.

(13) Ono, L. K.; Yuan, B.; Heinrich, H.; Cuenya, B. R. Formation and Thermal Stability of Platinum Oxides on Size-Selected Platinum Nanoparticles: Support Effects. *J. Phys. Chem. C* **2010**, *114*, 22119–22133.

(14) Steinberger, R.; Walter, J.; Greunz, T.; Duchoslav, J.; Arndt, M.; Molodtsov, S.; Meyer, D. C.; Stifter, D. XPS Study of the Effects of Long-Term Ar+ Ion and Ar Cluster Sputtering

on the Chemical Degradation of Hydrozincite and Iron Oxide. *Corros. Sci.* **2015**, *99*, 66–75.
(15) Rosado, G.; Verde, Y.; Valenzuela-Muñiz, A. M.; Barbosa, R.; Miki Yoshida, M.; Escobar, B. Catalytic Activity of Pt-Ni Nanoparticles Supported on Multi-Walled Carbon Nanotubes for the Oxygen Reduction Reaction. *Int. J. Hydrog. Energy* **2016**, *41*, 23260–23271.
(16) Godínez-Salomón, F.; Hallen-López, M.; Solorza-Feria, O. Enhanced Electroactivity for the Oxygen Reduction on Ni@Pt Core-Shell Nanocatalysts. *Int. J. Hydrog. Energy* **2012**, *37*, 14902–14910.